photonics

MDPI

Review

Multifunctional Smart Optical Fibers: Materials, Fabrication, and Sensing Applications

Zhengyong Liu [1,*], Zhi Feng Zhang [2], Hwa-Yaw Tam [1] and Xiaoming Tao [3,*]

1 Photonics Research Center, Department of Electrical Engineering, The Hong Kong Polytechnic University, Hong Kong, China; hwa-yaw.tam@polyu.edu.hk
2 College of Chemistry and Chemical Engineering, Ningxia Normal University, Guyuan 756000, China; 82016001@nxnu.edu.cn
3 Research Center for Smart Wearable Technology, Institute of Textiles and Clothing, The Hong Kong Polytechnic University, Hong Kong, China
* Correspondence: zhengyong.liu@connect.polyu.hk (Z.L.); xiao-ming.tao@polyu.edu.hk (X.T.)

Received: 22 March 2019; Accepted: 26 April 2019; Published: 6 May 2019

Abstract: This paper presents a review of the development of optical fibers made of multiple materials, particularly including silica glass, soft glass, polymers, hydrogels, biomaterials, Polydimethylsiloxane (PDMS), and Polyperfluoro-Butenylvinyleth (CYTOP). The properties of the materials are discussed according to their various applications. Typical fabrication techniques for specialty optical fibers based on these materials are introduced, which are mainly focused on extrusion, drilling, and stacking methods depending on the materials' thermal properties. Microstructures render multiple functions of optical fibers and bring more flexibility in fiber design and device fabrication. In particular, micro-structured optical fibers made from different types of materials are reviewed. The sensing capability of optical fibers enables smart monitoring. Widely used techniques to develop fiber sensors, i.e., fiber Bragg grating and interferometry, are discussed in terms of sensing principles and fabrication methods. Lastly, sensing applications in oil/gas, optofluidics, and particularly healthcare monitoring using specialty optical fibers are demonstrated. In comparison with conventional silica-glass single-mode fiber, state-of-the-art specialty optical fibers provide promising prospects in sensing applications due to flexible choices in materials and microstructures.

Keywords: specialty optical fibers; multi-materials; polymer optical fibers; soft-glass fibers; fiber Bragg grating; fiber sensors

1. Introduction

The advent of optical fibers with ultralow transmission loss (i.e., <0.18 dB/km) has enabled optical communication to develop rapidly and to connect the whole world with high-capacity networks. The key transmission medium that has played the most important role in this revolution is the single-mode fiber (SMF), which is made of silica glass and composed of a classic core and cladding. Basically, the refractive index of the core is slightly higher than that of the cladding, and light propagation obeys the principle of total internal reflection. To obtain such a fiber, an MCVD (Modified Chemical Vapor Deposition) process is needed to produce a preform containing the core and cladding at large scale, typically tens of mm in diameter and a few meters long. The fiber, with a diameter of 125 μm, is pulled from the preform, maintaining the diameter ratio of core to cladding. This type of fiber, called conventional SMF, has been widely used in communication systems and for sensing as well. The most common sensor configuration is based on the fiber Bragg grating (FBG) and is obtained by inducing a periodic index modulation in the core along the fiber using a UV laser [1]. Basically, when the FBG is subject to any perturbations of temperature, tensile strain, pressure, torsion, or other

parameters, the effective index of the fundamental mode in the core as well as the grating pitch will show corresponding changes, enabling the FBG to sense these physical parameters [2].

Besides silica glass materials, other thermally drawable materials have been proposed and demonstrated to fabricate optical fibers so that the fibers can be deployed with multiple functions. The first type of these materials is a polymer, such as polymethyl methacrylate (PMMA) [3], thermoplastic cyclic olefin copolymer (TOPAS®) [4], ZEONEX [5], PDMS [6], and hydrogels [7]. To achieve light guidance, either the core is doped with other materials to increase the refractive index, or microstructure is introduced [5]. Fiber made of polymer is especially flexible and biocompatible, making it a good candidate for medical applications. The other type of commonly used material to fabricate optical fiber is soft glass, e.g., chalcogenide glass [8] and telluride glass [9], which is a large group containing multiple materials and has low drawing temperature compared with normal silica glass. Typically, the soft-glass fiber is drawn at a temperature of hundreds of Celsius degrees depending on the constituents of the multiple materials, whereas silica-glass fiber is pulled at a temperature of ~1900–2100 °C according to the various structures or volumes of the preform. Due to the flexibility of the materials, the fiber can be made with step-index or gradient-index structure [10] or other microstructures [11]. These special fibers have been demonstrated for applications in supercontinuum generation [10], laser delivery [12], electric devices [13], microfluidics [14], fiber capacitors [15], sensing [16], and other fields. With the introduction of novel materials, the function of optical fibers could be greatly enhanced beyond that of conventional optical communication.

Figure 1 summarizes the development and applications of multi-material optical fibers. Compared with conventional silica-based fibers, these fibers provide more options to incorporate different kinds of materials such as chalcogenide glass, semiconductor materials, and even metals. Polymer optical fibers, also offer choices instead of the classic PMMA, for example, TOPAS, ZEONEX, PDMS, and some hydrogels. Because of the flexibility of incorporating all these materials, more novel functions have been developed based on the form of optical fibers.

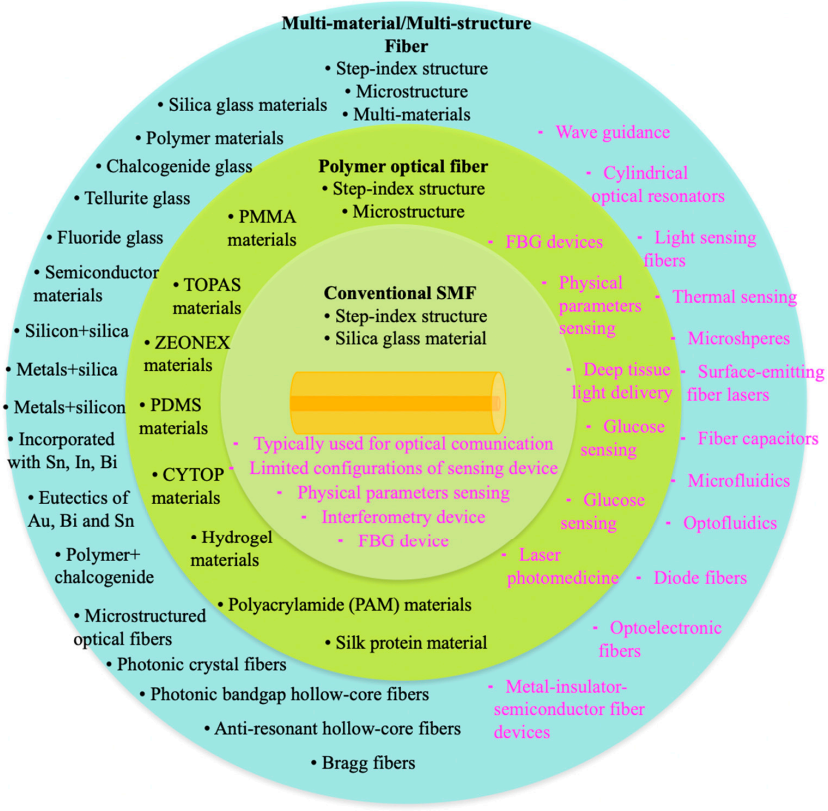

Figure 1. Summary of typical materials and functions for conventional SMF, polymer optical fibers, and multi-material fibers.

This paper provides a comprehensive review of the development of state-of-the-art optical fibers based on various materials, including silica glass and polymers. Section 2 presents typical materials used for specialty optical fibers as well as fabrication methods, followed by the introduction of microstructures to the fiber in Section 3. Section 4 describes the widely used techniques for fiber sensor development, including the principle and fabrication of the fiber Bragg grating. Section 5 presents interferometric sensing techniques. In Section 6, sensing applications based on specialty optical fibers are presented. Finally, conclusions are drawn, and some prospects for multi-material fibers are presented.

2. Materials and Fabrication Methods

2.1. Silica Glass-Based Fibers

Silica glass has been used to fabricate SMFs or multimode fibers (MMFs) in the preform-drawing process. First, a preform is produced using MCVD technology, focusing on the deposition of core materials, e.g., silica doped with germanium, ytterbium, erbium, bismuth, and so forth. Germanium dopant is very common because it can increase the refractive index of the core region. Due to the presence of Ge, the fiber is photosensitive to UV light, enabling it to be inscribed with Bragg gratings [17]. Different dopants in the core lead to various applications. For example, ytterbium and erbium are used to enable emissions to be excited by pumping light, which is used for fiber lasers and amplifiers. Similarly, thulium is introduced to scale up the power of a fiber laser as well as the lasing wavelength [18]. To develop high-power fiber lasers, the challenging issue is to increase the lasing power by doping higher concentrations of active materials, but at the same time reducing photo quenching and nonlinear effects to their lowest possible levels. When the dopant concentration is increased, the molecules tend to cluster, affecting the absorption efficiency of pumping light. To reduce cluster formation, aluminum and phosphorus are used [19]. Aluminosilicate or phosphosilicate fibers are two common substrates for heavy dopants because Al or P can increase core solubility during preform fabrication. By using such a strategy, Ramírez-Martínez et al. demonstrated that a heavy Tm concentration of ~5.6 wt% can be doped uniformly into the core and incorporated with high Al_2O_3 as well, leading to a high slope efficiency of >70% [20].

Apart from doping active ions into the fiber core to develop high power fiber lasers, micro-structured optical fiber (MOF) is another type of specialty optical fiber that can be fabricated using only a single material like silica glass. Typically, MOFs rely more on microstructures that introduce functions to the fiber rather than on the materials used. Photonic crystal fiber (PCF), one famous kind of MOF, is such an optical fiber that has air holes arranged in a hexagonal or square lattice along the fiber length [21]. Basically, PCF is made of pure silica glass, and the light guidance obeys two new mechanisms: modified TIR (M-TIR) and photonic bandgap (PBG). A detailed description of micro-structured fibers is presented in Section 3.

The drawing temperature of conventional silica glass is around 2000 °C. The softening temperature of silica glass is around 1600 °C. As the temperature keeps increasing, the glass materials start to melt until they can be pulled by external force. A capstan is used to pull the fiber with a certain tension, which is determined by drawing speed and temperature. One key parameter to be controlled is the viscosity of the silica glass. Because air holes exist in MOFs, the drawing temperature is lower than with all-solid silica fibers. The relatively lower temperature, typically about 1900 °C, serves to maintain the air-hole structure during the drawing process [22]. This rule is applicable to all types of MOFs made of various materials, e.g., polymers or soft-glass materials.

2.2. Soft Glass-Based Fibers

Soft glass is a group of materials that have lower melting temperature than conventional silica glass. Typically, the drawing temperature of soft glass varies from 200 °C to 1000 °C, depending on the constituent materials. Chalcogenide glasses (e.g., As_2S_3 [23] and As_2Se_3 [24]) are commonly used

because they can be easily incorporated with other components like Ge, Sn, Te, and other semiconductor materials. The greatest benefit of using chalcogenide glass materials is the ability to transmit in the mid-IR region covering a range from ~2 μm to ~14 μm. Within this IR regime, this type of fiber can be a good platform for biomedical and industrial applications. Due to the high nonlinearity of chalcogenide glass, this type of fiber is widely used to generate a supercontinuum. With a step-index structure where the core and cladding have slightly different constituents, the broadband light generated can range from 1.5 μm to 14 μm [25]. The core is made of $Ge_{20}As_{20}Se_{15}Te_{45}$, and the cladding is $Ge_{20}As_{20}Se_{17}Te_{43}$. To make a preform of this fiber, the extrusion method is used because the material has lower melting temperature. Moreover, the same group also reported the MIR supercontinuum covering from 2–16 μm in a low-loss tellurite SMF, which is the broadest supercontinuum generation reported in the normal dispersion regime [9].

Because soft glass is more flexible than silica glass, typically with a Young's modulus of 10–20 GPa [26], it can be used for biomedical sensing applications as well. Biochemical analysis is a very promising application of chalcogenide optical fibers [8,27,28]. The absorption peaks of the biomedical molecules normally appear in the mid-IR regime. The chalcogenide fibers can support this wavelength band with very low attenuation. Some FBGs have been inscribed on chalcogenide fibers to develop grating-based devices, including sensors. Unlike FBGs written on silica-glass fibers using core photosensitivity only, the core and cladding of chalcogenide fibers are both sensitive to 633 nm laser light [23,29]. The grating form is different as well, meaning that refractive index modulation is induced in both core and cladding. In addition to all-solid chalcogenide fibers, micro-structured optical fibers can be fabricated, e.g., PCFs. To introduce microstructures into the fiber, normally the drilling method is used [30]. This is the most straightforward approach to obtain the desired structure. However, during the drawing process for chalcogenide PCF, the temperature must be controlled more precisely than for silica-glass PCF because the viscosity of chalcogenide materials changes quickly even if the temperature fluctuates by about 20–30 °C. Polarization-maintaining fiber is possible by introducing two larger holes adjacent to the center core, similarly to the polarization-maintaining PCF (PM-PCF) based on silica glass, or by introducing other asymmetrical structures. The birefringence of such fiber can easily reach 1.5×10^{-3} [11].

2.3. PMMA POFs

PMMA is one of the most widely used optical polymers for POFs and has a refractive index of 1.49. Traditional step-index POFs have a PMMA cladding and a PMMA core with dopants. Nevertheless, attenuation of PMMA fibers is a few orders of magnitude higher than that of silica-glass fibers. Commercial PMMA-based POFs are fabricated by the co-extrusion process because it is continuous and highly autonomous.

PMMA is also the material of choice for fabricating photosensitive single-mode POFs, which are used for inscription of fiber Bragg gratings in most present studies [31–33]. In contrast to commercial POFs, almost all single-mode POFs are made by the preform-drawing method in research laboratories [34,35]. A cladding of PMMA or copolymers of methyl methacrylate and other acrylate monomers is prepared by radical polymerization. Then the PMMA core doped with small photosensitive organic molecules is polymerized. Finally, the preform is thermally drawn to fibers of the desired diameters using a fiber drawing tower. The key to the fabrication process is to tune the refractive index difference between the fiber core and cladding and to control the diameter of the fiber core so that the produced fiber supports only single-mode transmission. In addition, PMMA is used to make micro-structured POFs, which are normally fabricated by drilling holes in a designed pattern into the preform and then thermal drawing [36], or by stacking PMMA rods/tubes to form a preform and then thermal drawing [37]. In addition to PMMA, thermoplastic cyclic olefin copolymer (TOPAS®) has been used to make micro-structured POFs in the past few years [4,38]. The key feature of TOPAS is its extremely low water absorption, which makes its fibers humidity-insensitive.

2.4. Biopolymer Optical Fibers/Waveguides

Some soft biopolymer hydrogels have been widely used in biotechnology because of their excellent softness and biocompatibility. In the past few years, such soft polymers have been developed as optical materials. They are made into optical fibers or waveguides for a wide range of advanced and interesting applications. Those hydrogels includes poly(ethylene glycol) diacrylate (PEGDA) [7,39,40], polyacrylamide (PAM) [41–43], silk protein [44,45], agarose [46,47], poly(lactic acid) (PLA) [48], alginate [39], and copolymers like poly(acrylamide-co-poly(ethylene glycol) diacrylate) p(AM-co-PEGDA) [49], as listed in Table 1.

Table 1. Soft biopolymer-based optical fibers and waveguides.

Type	Materials	Fabrication Method	Application	Reference
Fiber	Core: poly(octamethylene maleate citrate) Cladding: poly(octamethylene citrate)	Cladding tube cured around a steel mold, core solution infiltrated into the cladding and crosslinked	Deep tissue light delivery, fluorescence sensing, laser photomedicine	[50,51]
Fiber	Core: poly(acrylamide-co-poly(ethylene glycol) diacrylate) Cladding: Ca alginate	Core crosslinked in a tube mold and ejected. Cladding by dip-coating in alginate solution.	Glucose sensing	[49]
Fiber	Core: spider silk protein No cladding	Core crosslinked in a tube mold	Deep tissue light delivery	[45]
Waveguide	Core: carbon dot-doped PEGDA No cladding	Photo-crosslinked in mold	Detection of heavy metal ions	[50]
Waveguide (splitter)	Core: bovine serum albumin No cladding	Core film crosslinked, then splitter fabricated by laser writing	Optic splitter	[52]
Waveguide	Core: poly(L-lactic acid); PEGDA; silk protein	Melt-pressing; photo-crosslinking; solution-casting	Deep tissue light delivery	[48]
Fiber	Core: alginate-polyacrylamide No cladding	Core photo-crosslinked in a tube mold; cladding by dip-coating	Strain sensing	[42]
Fiber	Core: PEGDA Cladding: Ca2+ alginate	Core photo-crosslinked in a tube mold; cladding by dip-coating	Deep tissue light delivery and sensing	[39]
Waveguide	Core: PEGDA No cladding	Slab waveguide photo-crosslinked	Deep tissue light delivery and collection	[7]
Waveguide	Core: Agarose Cladding: Agarose	Cladding substrate solution casted; Core created by lithography	Cell encapsulation and	[46]
Waveguide	Core: silk No cladding	Direct ink writing	-	[44]

2.5. Elastomer Optical Fibers/Waveguides

Polydimethylsiloxane (PDMS) is optically clear and has excellent elastic deformability and biocompatibility. It has been used for contact lenses among a large number of applications. By taking advantage of its superior properties, PDMS has been used to fabricate stretchable optical fibers and waveguides, as listed in Table 2. Other transparent elastomers being used to fabricate stretchable optical fibers include polyurethane [53] and polystyrene-based polymers [6].

Table 2. PDMS-based optical fibers and waveguides.

Type	Materials	Fabrication Method	Application	Reference
Fiber	Core: PU Cladding: PDMS	Commercial core, solution-coating cladding	Fibers attached to textiles for >100% strain sensing	[54]
Waveguide	Core: PDMS (ELASTOSIL M 4601, n: ~1.40) Cladding: Polyurethane (VytaFlex 20, n: ~1.46)	Soft lithography	As touch sensor for the fingertip of a prosthetic hand	[53]
Waveguide	Core: Silicone (Nusil Technology LS-6257, n = 1.57) Cladding: PDMS (Dow Sylgard®184, n = 1.41)	Cladding made first and core prepolymer was injected (capillary filling) and cured	n/a	[55]
Fiber	Core: Silicone (Nusil Technology LS-6941) No cladding	Drawing of sticky pre-polymer	n/a	[56]
Fiber	Core: polystyrene-based polymer (Star Clear, n = 1.52) Cladding: fluorinated polymer Daikin T-530 (n = 1.36)	Continuous coextrusion, fibers up to several hundred meters	Sensing strain up to 300%	[6]

2.6. Multi-Material Multifunctional Fibers

Multi-material multifunctional fibers were pioneered by the research group headed by Prof. Yoel Fink from MIT [57]. The group has developed highly sophisticated fiber devices and has advanced fibers to new frontiers. These fibers fulfill not only optical, but also optoelectronic functions because of their multiple-component fiber structure as well as their great application potential.

Such fibers may be composed of low-melting-temperature metal, inorganic glass, polymer, and even microelectronic chips and other components. Different materials and components are arranged in concentric circles to form macroscopic preforms, which are thermally drawn into fibers. In addition, such fibers can be woven into fabrics to realize multifunctional smart fabrics. The key of selecting and integrating these materials is to choose components with similar melting or glass transition temperatures so that they can be co-drawn. The researchers selected chalcogenide glasses as the main inorganic material, which contain one or more of the chalcogen elements (e.g., sulfur, selenium, and tellurium). They have glass-transition temperatures between 100 and 400 °C. The polymers include polyether sulfone (PES), polysulfone (PSu), and polyether imide (PEI). Metals with low melting points, like Sn, In, Bi, or their alloys, are incorporated into chalcogenide glass to make optoelectrical devices based on a fiber form.

Fink et al. designed preforms in various configurations by using two or more materials and fabricated the fibers with desired functions, including hollow photonic bandgap fibers for wave guidance [58,59], cylindrical optical resonators [60,61], light-sensing fibers [62], self-monitoring fibers [63], thermal sensing fibers [16], surface-emitting fiber lasers [64], fiber capacitors [15], microfluidic fibers [14], and diode fibers [65].

2.7. Polyperfluoro-Butenylvinylether (CYTOP®) POFs

CYTOP, innovated by Asahi Glass Co. (Tokyo, Japan), is an amorphous perfluorinated polymer and has better transparency and lower losses than PMMA. It is mainly used as the core of graded-index POFs with low loss. Commercial CYTOP fibers have a loss of approximately 10 dB/km within the standard communication wavelength band (800–1300 nm).

Taking advantage of its excellent properties, researchers have also used CYTOP for UV waveguides [66] and Bragg gratings [67]. FBGs have been successfully written onto commercial multi-mode graded-index CYTOP fibers [68]. CYTOP has low losses and poor affinity for water, properties that are superior to PMMA, making FBGs based on CYTOP fibers less influenced by humidity and hence more appealing for sensing applications.

3. Multifunctional Microstructures in Optical Fibers

Microstructures can be introduced into all kinds of optical fibers made of different materials. The introduced microstructures modify both the mechanical and optical properties of the fiber, making it a good platform for multifunctional devices. According to the material type, various techniques are used to fabricate the microstructures, including drilling [30], extrusion [69], and stacking [70]. Normally, drilling air holes in a preform is limited by machining precision as well as the length of the drill bit. The drilling process affects the roughness of the inner surface of the structure, whereas the length of the drill bit determines the total length of the preform, which eventually affects the fiber length to be drawn. The extrusion method enables the fabrication of air-hole structures in soft-glass or polymer materials due to their low melting temperature. Typically, the shape of the microstructure depends on the extrusion die used. The die is machined precisely according to the designed fiber structure. In such a way, the fiber can be made with very tiny structures, e.g., subwavelength suspended-core fiber [71]. Ideally, the extrusion method can accommodate any type of microstructure as long as the corresponding die can be machined. On the other hand, different materials can be co-extruded to make core and cladding layers simultaneously [72]. Recently, the anti-resonant MOF has been widely investigated because of its superior performance in light delivery [73]. When the stacking method is used, the structure is very limited; for example, it is difficult to obtain good negative curvature structure with more inner rings [74]. Due to the flexibility of the extrusion die, creating such microstructures is possible and easy, such as the successful demonstration of a negative-curvature fiber with one ring of air holes [75]. However, the limitations of the extrusion process are also very prominent. The process requires a low melting temperature of the constituent material, normally less than 1000 °C.

Another widely used technique to fabricate MOFs is stack-and-draw, which includes preparing a preform by stacking the desired structures using capillaries and drawing fiber from the stacked preform. It was initially invented to fabricate PCFs [76], including index-guiding as well as hollow-core PCFs. The advantage of the stacking method is that it can be used for any kind of material regardless of melting temperature. Many capillaries are first drawn from a large tube of the required material. Then those capillaries with identical or different dimensions are used to stack the air-hole structure of the PCF or of other types of MOFs [77]. Apart from the PCFs with hexagonal air-hole structure that have been demonstrated, MOFs with suspended core [78], semicircular holes [79], "butterfly" structure [80], and super-lattice structure [81] have been successfully fabricated using this technique. Because of the flexibility of the stacking method, almost any kind of microstructure with any material can be made in this manner. However, when the air-hole structure includes different sizes, the air holes may deform seriously due to unbalanced pressure during drawing. Generally, this issue exists for all methods of making special MOFs. Therefore, the drawing conditions, such as drawing temperature, drawing speed, and tension, must be optimized and controlled carefully to achieve the desired microstructure.

Figure 2 schematically shows the MOF fabrication processes described above. The difference among these techniques is mainly in the preparation of the preforms. Fibers based on different materials can be made using various methods.

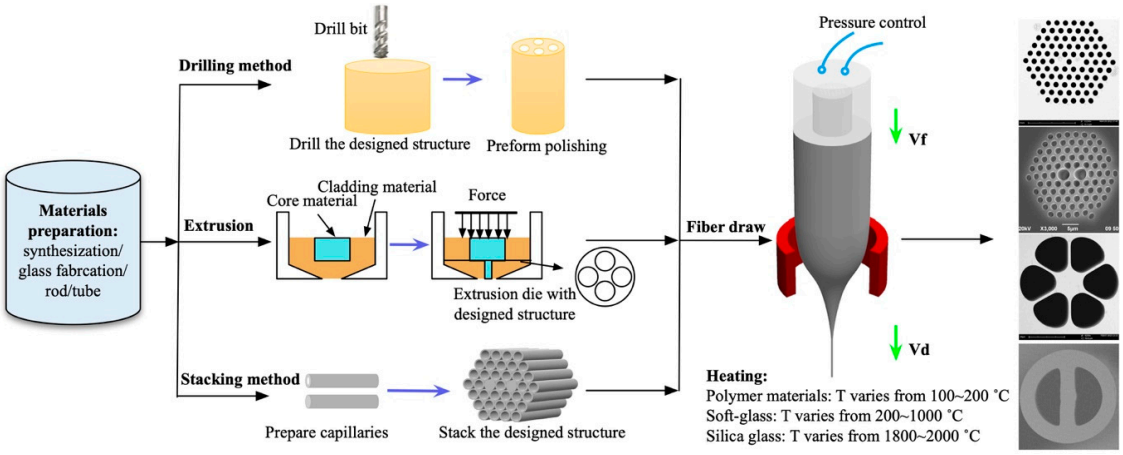

Figure 2. Schematic of MOF fabrication using drilling, extrusion, and stacking methods.

4. Fiber Grating Technology

4.1. Sensing Principle

Currently, the fiber Bragg grating (FBG) is widely used in many areas such as filters, dispersion compensators in communication, sensors, and reflectors for fiber lasers. The photo-elastic and thermo-optic effects are used for sensing. External perturbations such as strain, pressure, vibration, and temperature lead to changes in optical properties (i.e., the refractive index), mechanical properties, and dimension (i.e., deformation) of the materials, which eventually appear as a shift in the Bragg grating peak. The Bragg wavelength of single-mode optical fibers can be expressed as:

$$\lambda_B = 2n_{eff}\Lambda \tag{1}$$

where n_{eff} is the effective index of the fundamental mode in the fiber and Λ represents the pitch of the FBG written in the fiber. When the FBG is subjected to a perturbation in the environment, the change will cause corresponding variations in n_{eff} and Λ. The relationship can be formulated as [2]:

$$\frac{\Delta\lambda_B}{\lambda_B} = \left\{1 - \frac{{n_{eff}}^2}{2} \cdot [P_{12} - v(P_{11} + P_{12})]\right\}\varepsilon + \left(\alpha + \frac{1}{n_{eff}}\frac{dn_{eff}}{dT}\right)\Delta T \tag{2}$$

where P_{11}, P_{12} are the stress-optic coefficients, v is Poisson's ratio, α is the coefficient of thermal expansion (CTE), and ε and ΔT are the strain and the temperature change. As for the standard silica SMF, the factor $\frac{n_{eff}^2}{2}[P_{12} - v(P_{11} + P_{12})]$ can be numerically estimated as 0.22. In practical terms, the Bragg wavelength shift induced by external perturbation is mainly related to the effective index change (Δn_{eff}) and the pitch change ($\Delta\Lambda$), which can be expressed as:

$$\frac{\Delta\lambda_B}{\lambda_B} = \frac{\Delta n_{eff}}{n_{eff}} + \frac{\Delta\Lambda}{\Lambda} \tag{3}$$

According to Equation (3), the corresponding Bragg wavelength shift caused by a certain perturbation (e.g., pressure, ΔP) can be obtained theoretically by calculating the effective index and the pitch change. The value of $\Delta\lambda_B/\Delta P$ is the theoretical sensitivity. Using this approach, simulation and experimental results can be compared [82].

Apart from axial strain measurement, the FBG can be used to detect lateral compression strain [83]. Model coupling occurs in fiber gratings [84], which can be used to achieve simultaneous multiple-parameter measurements. Hybrids of FBG with other gratings form a range of superstructured fiber gratings such as long-period grating and chirped grating. For instance, a pair of FBGs separated

by a cavity [85] or an FBG with a tapered cavity [86] can be used for simultaneous measurements of fiber axial strain and temperature. Cladding mode recoupling in a concatenated LPG and FBG [87] or a step-changed LPG [88] has been used for simultaneous measurement of axial strain, transverse pressure, and temperature [89].

4.2. Fabrication Techniques

Photosensitivity is necessary to inscribe FBGs on a single fiber. For a silica-glass based fiber, the core is typically doped with germanium to increase the core index. The coincidence is that this dopant also introduces photosensitivity to the fiber, thus enabling FBGs to be inscribed on the standard SMF/MMF. Typically, to obtain strong FBGs, the SMF is loaded in a chamber with hydrogen under high pressure for some time to enhance its photosensitivity [90]. There are two main approaches to writing FBGs: one uses interferometry and the other a phase mask [91]. The former method uses the interference pattern of two laser beams to write the gratings. The grating pitch on the fiber is related to the interference angle of the two laser beams, which means that the grating pitch can be tuned easily and freely simply by adjusting the angle. However, this technique requires very precise optical alignment so that the interference pattern can be printed exactly onto the fiber. Much effort is needed, especially after adjusting the angle, making mass production of FBGs difficult. In contrast, the phase-mask technique is more versatile and easier to handle. The grating pattern is also induced from two interfering laser beams, but the two beams are diffracted from a single phase mask. The fiber is typically placed just behind the phase mask. In this way, the pitch of the FBG is half the pitch of the grating on the phase mask. Therefore, one phase mask with a certain pitch determines one FBG. Advantages are that the fabrication process is simple, stable, and repeatable, which is desirable for mass production. Nevertheless, to fabricate more FBGs with different pitches requires more phase masks. Because the phase mask can be used many times, this is still a favorable cost-effective approach to inscribing FBGs.

The essential requirement for writing FBGs is the laser, which can be a UV laser, a red laser, a femtosecond laser, a CO_2 laser, or another type depending on the constituent materials. UV lasers have wavelengths of 193 nm [92], 213 nm [93], 248 nm, 266 nm, or 325 nm. Shorter wavelength means higher energy. For silica glass-based fiber, 193 nm, 213 nm, 248 nm, and 266 nm lasers are used because the Ge-doped core is photosensitive to such wavelengths and the reflective index can be modulated by the laser. A 325 nm laser is typically used to inscribe FBGs on polymer optical fiber, especially PMMA-based POFs. Because polymers are soft and some are photosensitive over a broad UV range, UV lasers emitting at 193 nm or 248 nm can also be used to make gratings provided that periodic modulation (e.g., in refractive index or in physical deformation) can be induced [94]. A red laser at 633 nm is good for chalcogenide fibers because this material (e.g., As_2Se_3) is photosensitive to this wavelength [29]. When using femtosecond lasers, almost any grating can be fabricated regardless of material type due to much-reduced thermal effects. In most cases, the femtosecond laser induces physical damage or deformation to the fiber, forming the grating structure. The wavelength of such femtosecond lasers is typically at ~800 nm [95] or ~1030–1060 nm [96], but the laser has high energy. UV femtosecond lasers are also used to write FBGs, e.g., 400 nm [97], which can induce index change as well because of photosensitivity.

Figure 3 shows a schematic of the FBG inscription setup using a phase mask and a Talbot interferometer. These two techniques are widely used in research and industry. The lasers in the setup can be any of those mentioned above, and the fibers can be MOFs, PCFs, POFs, or soft-glass fibers. Different materials respond differently to the lasers, but the configuration is similar. One exception is the technique of point-by-point exposure using femtosecond lasers, where the grating pattern is written by the laser point by point with high precision of laser movement and good control of the laser spot. Typically, the beam size of the femtosecond laser can be focused to hundreds of nanometers, enabling it to conduct micromachining, including grating inscription with complex profile and positioning [98]. For polymer and soft-glass fibers, the femtosecond laser is a good option to

inscribe FBGs and long-period gratings (LPGs). Because of its powerful capabilities, other types of microstructures can be micromachined directly onto the fibers. For example, multiple cores with individual FBGs can be created directly using only the femtosecond laser on an SMF [99]. In this scenario, other waveguides can be created in the cladding by the laser, and FBGs are inscribed on the core simultaneously. Similarly, other kinds of desirable microstructures can be created in fibers made of, e.g., polymers or chalcogenide glass.

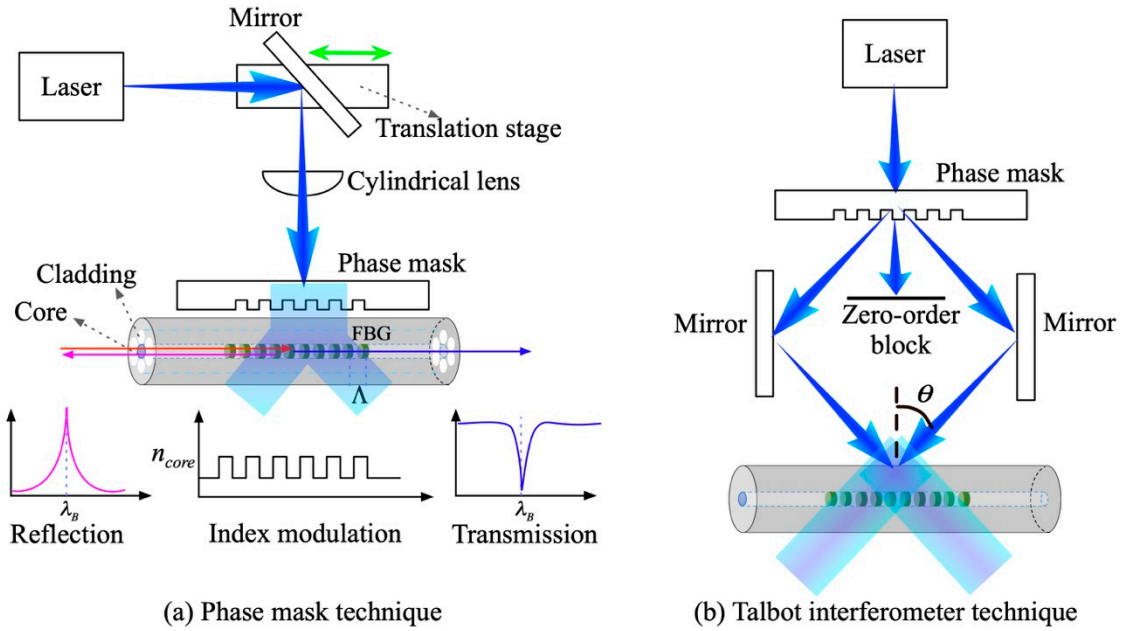

Figure 3. Schematic of the FBG inscription setup based on (**a**) the phase-mask technique and (**b**) the Talbot interferometer technique.

5. Interferometric Technology

Apart from the FBG used to develop the fiber sensors, the interferometer is another commonly used structure. Typical models include the Fabry-Perot interferometer (FPI), the Mach-Zehnder interferometer (MZI), and the Sagnac interferometer (SI). All these structures have two separate light paths that interfere constructively or destructively depending on the phase difference between them. Figure 4 illustrates the schematic configurations of three typical interferometers.

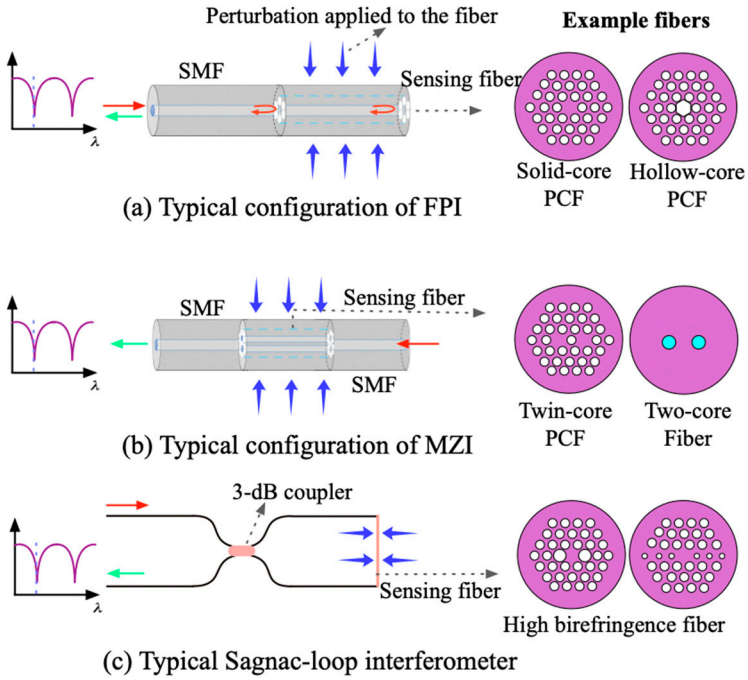

Figure 4. Typical configurations of FPI, MZI, and SI interferometers.

In particular, to form an inline interferometer on a fiber, the two optical paths are realized using multiple cores, different modes guided in the core, or two counter-propagating modes. As for the FPI shown in Figure 4a, the FP cavity can be constructed by placing a solid-core PCF [100], a hollow-core PCF [101], or another hollow fiber between two SMFs. The interference occurs between the reflections from the first and second facets of the FP cavity. Therefore, the phase difference (φ) can typically be expressed as:

$$\varphi = \frac{4\pi}{\lambda} n_{eff} \cdot L \tag{4}$$

where n_{eff} is the effective index of the fundamental mode guided in the FP cavity and L is the cavity length. In the MZI configuration, the interference is typically formed by two waveguides, e.g., two cores in a fiber [102], or two guiding modes, e.g., a two-mode fiber [103].The propagation constants of the fundamental mode guided in each core are different, depending on the fiber design. The phase difference of MZI can be formulated as

$$\varphi = \frac{2\pi}{\lambda}\left(n_{eff,1} - n_{eff,2}\right) \cdot L \tag{5}$$

where $n_{eff,1}$ and $n_{eff,2}$ are the effective indices of the fundamental mode guided in the two cores individually and L is the length of the specialty optical fiber.

Unlike FPI and MZI, SI can be configured only by using an optical fiber with high birefringence regardless of the material used. Birefringence is the refractive index difference between the two orthogonal modes supported in the fiber, i.e., $B = |n_{eff,x} - n_{eff,y}|$ [104]. Typically, this type of fiber is called a polarization-maintaining fiber (PMF). A PMF can also be created by introducing an asymmetrical air-hole structure, for example, a PM-PCF [105], a polarization-maintaining hollow-core fiber [106], a high-birefringence suspended-core fiber (HB-SCF) [78], or two semicircular side-hole MOFs [79]. Figure 4c shows a typical SI configuration using PMF. The 3-dB coupler splits the broadband light into two counter-propagating beams, which interfere constructively or destructively at the same coupler after transmission through the PMF. The phase difference in SI arises from the two orthogonal polarizations and can be expressed as:

$$\varphi = \frac{2\pi}{\lambda} B \cdot L \tag{6}$$

When the inline interferometers are subjected to perturbations caused by the measurands, e.g., temperature, strain, pressure, or vibration, the phase difference changes correspondingly, eventually resulting in a blue or red shift in the interference spectrum. Normally, when tracking the shift of the wavelength dip in the interference spectrum, the phase difference at the dip is always equal to $2k\pi$ (k an integer) [107]. Therefore, the corresponding sensitivity of FPI, MZI, and SI can be deduced as Equation (7):

$$\frac{d\lambda}{dX} = \frac{\lambda}{n_g}\frac{dn_p}{dX} + \frac{n_p}{n_g}\frac{\lambda dL}{LdX} \tag{7}$$

where X represents the measurand to be sensed and n_p, n_g are the phase and group indices of the two interference beams, corresponding to the propagation constant and the dispersion effect respectively. In particular, n_p and n_g are the phase and group effective indices of the fundamental mode guided in the FP cavity. With MZI and SI, the index difference of the two light beams should be accounted for, i.e., $n_p = n_{eff,1} - n_{eff,2}$, $n_g = n_{eff,1,g} - n_{eff,2,g}$ for MZI, $n_p = B$, $n_g = G$ for SI. For sensing cases where the fiber length does not change significantly, the second item of Equation (7) can be removed after ignoring the length effect. Basically, the sensing performance evaluated by Equation (7) is based on the changes in refractive index and fiber length caused by the photo-elastic effect and the thermo-optic effect respectively. Using such an approach, interferometric sensors can be developed and evaluated.

6. Sensing Applications

6.1. Pressure Sensing Based on the FBG and Interferometry

There is a great need for sensing in the oil and gas industry because real-time monitoring of oil pressure and flow rate plays a vital role in controlling production and transport. In addition, this feedback is important for safety. To develop pressure sensors with different performance levels, the FBG and interferometric techniques described above are commonly used. Figure 5 provides a schematic of an optical fiber sensing system application in the oil industry. The multiplexing and long-distance measurement capabilities of this system make it promising for remote monitoring, especially in the extreme downhole environment. Taking the oil pressure measurement as an example, the sensitivity using an FBG written on a conventional SMF is only ~4 pm/MPa [108], which is insufficient for precise pressure management. It is hard to obtain substantial improvements in sensitivity using only SMF because mechanical deformation is very limited due to the all-solid structure. In contrast, MOFs can provide better flexibility to control the stress distribution induced by external pressure. For FBG-based pressure sensors, the sensitivity can be improved to ~13 pm/MPa by using a six-hole suspended-core fiber [109]. This is already a substantial improvement compared with the conventional SMF. However, by introducing larger air holes into the fiber, meaning a higher air-filled fraction, the sensitivity can be further enhanced to ~44 pm/MPa when using an FBG written on a single-ring suspended fiber [82]. The fiber possesses a large air region in the cross section, and the air-filled fraction can be as high as 65%. This is the highest pressure sensitivity that has been demonstrated for silica FBG-based sensors. With the introduction of microstructure to the fiber, the performance of pressure sensors can clearly be much improved. The reason for this is that the microstructure reduces the rigidity of the fiber, causing larger axial strain to the core. Meanwhile, the refractive index does not change very much because of the suspended structure. Both factors lead to a larger blue shift of the Bragg wavelength under a certain pressure. These results are based on silica-glass fibers. Polymer optical fiber is also a good option for pressure measurement, and higher sensitivity is expected because this material has much lower Young's modulus. The demonstrated pressure sensitivity is up to ~200 pm/MPa for a POF Bragg grating [110].

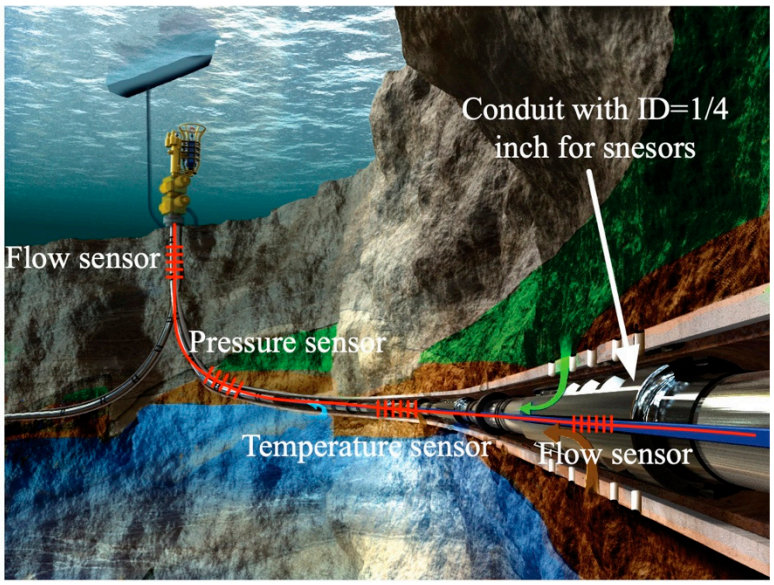

Figure 5. Schematic of a fiber optic sensing system for submarine oil exploitation (permission obtained from [111]).

In addition to the FBG-based approach, another type of interferometer is used as well to perform pressure measurements. The Sagnac interferometer is a widely used configuration because it uses the polarimetric effect, typically depending on the difference between two MOF polarization states. In this case, the advantage of MOFs is obvious because of the flexibility of their air-hole arrangement to introduce birefringence. The first pressure measurement demonstrated using SI based on PM-PCF showed a pressure sensitivity of 3.42 nm/MPa [112]. By detecting the pressure-induced birefringence difference of two polarization states in PM-PCF, the sensitivity can be increased to about 1000 times that based on FBG in SMF. This PM-PCF consists of uniform air holes arranged within a hexagonal structure, and the birefringence is introduced by enlarging two air holes adjacent to the core. The geometrical difference between the two polarization axes is very limited, especially when the fiber is subject to external perturbations such as pressure change. Other microstructures are then developed to enhance pressure measurement performance further, for instance, the "butterfly"-type MOF [80], the semicircular-hole MOF [79], and the side-hole fiber [113]. Among these special microstructures, the highest pressure demonstrated with the SI configuration was based on the semicircular-hole MOF, showing a sensitivity up to ~50 nm/MPa and a large dynamic range of 116 dB [79]. Table 3 lists the state-of-the-art specialty optical fibers developed for pressure measurement and their corresponding performance.

Low pressure measurement (<40 kPa) is necessary for monitoring human activity and physiological parameters. As shown in Table 3, the sensitivity of many optical fiber sensors cannot provide satisfactory results in this region. Structural conversion is an effective method that raises the pressure sensitivity using a specific sensor structure where the optical fiber is used as the sensing element. For example, a high sensitivity of 820 pm/kPa was achieved by structure conversion in this low-pressure region [114].

Table 3. Comparison of specialty optical fibers developed for pressure measurement and their performance.

Type	Sensing Principle	Pressure Sensitivity	Reported Year	Reference
SMF	FBG	3.1 pm/MPa	1993	[108]
High-birefringence side-hole fiber	FBG	−1.93 pm/MPa for $LP_{01}{}^{x}$ and −5.37 pm/MPa for $LP_{01}{}^{y}$	2003	[115]
Carbon fiber ribbon-wound composite cylindrical shell	FBG	452 pm/MPa	2009	[116]
"Grapefruit" MOF	FBG	12.8 pm/MPa	2010	[109]
Micro-structured POF	FBG	130 pm/MPa	2012	[117]
"Butterfly"-type MOF	FBG	33 pm/MPa	2012	[118]
Single-ring suspended fiber	FBG	44 pm/MPa	2019	[82]
POF	FBG	200 pm/MPa	2015	[110]
Few-mode fiber	Mode interferometer	−23.7 pm/MPa	2011	[103]
Index-guiding PCF	Fabry-Perot interferometer	−5.8 pm/MPa	2011	[100]
Twin-core PCF	Supermode interferometer	−21 pm/MPa	2012	[119]
PM-PCF	Sagnac interferometer	3.42 nm/MPa	2008	[112]
High-birefringence suspended core fiber	Sagnac interferometer	2.82 nm/MPa	2014	[78]
Elliptical-core side-hole fiber	Polarimetric (Sagnac interferometer)	~26 nm/MPa	2016	[120]
Capillary fiber with an embedded core	Polarimetric (Sagnac interferometer)	10.4 nm/MPa	2017	[121]
Semicircular-hole MOF	Sagnac interferometer	~50 nm/MPa	2018	[79]
Silicone structured POF sensor	POF FBG	820 pm/kPa	2013	[114]

6.2. Optofluidic Sensing Based on Multifunctional MOFs

Optofluidics is a multidisciplinary field that studies the interaction between microfluidics and light. Physical contact between the light and the substance is essential. Normally, specially designed biochips integrated with optical fibers are used, where the fibers function as light waveguides [122]. Based on lab-on-a-chip or lab-in-fiber device technologies, many applications have been demonstrated, for example, chemical analysis, particle sorting, and bioanalysis, as well as biosensors for detection of DNA, refractive index, and microfluidic flow rate. A complete review of optofluidics can be found in [123].

Microfluidic chips are more popularly used to conduct optofluidics because microchannels can be fabricated easily on a single chip, enabling fluids to pass through. Micro-structured optical fibers that already have air-hole channels along the fiber length provide another way to conduct optofluidic measurements Using MOFs, the air holes act as microfluidic channels for the analytes to flow through while the optical core guides the light [124]. Due to the unique guiding mechanism of the PCF photonic bandgap, a hollow-core PCF is also possible, meaning that the light propagates in the channel. This enables liquid to flow in the core, enhancing the light-matter interaction. Using this technology, many optofluidic devices on MOFs have been demonstrated [125], such as refractive index measurement [124], photochemical reaction analysis [126], and catalytic microreactors [127]. To enable liquids to flow into MOF microchannels, multiple approaches can be used, for example, using a femtosecond laser to drill

side holes [128], connecting a C-shaped fiber [124], and designing a special adapter between SMF and MOF [126]. Furthermore, soft-glass multimode fiber with high numerical aperture thanks to its high refractive index can be used to conduct particle manipulation in three dimensions [129], which is very promising for optical tweezers. Even though many optofluidic devices demonstrated are based on silica-glass fibers, similar concepts can be used for polymer- or soft glass-based fibers as long as the fiber contains the desired microstructures.

6.3. Health Monitoring and Promotion

Health monitoring is undoubtedly important, and monitoring is becoming smarter and easier. Typically, health-care monitoring includes vital signs measurements such as heart rate, respiration, blood pressure and sugar, and ballistocardiograph (BCG) readings. Real-time monitoring of these vital signs is very necessary for patients in recovery or under magnetic resonance imaging (MRI). Therefore, people have invented smart textiles embedded with optical fiber sensors to enable health-care monitoring [130]. Wearing smart textiles during monitoring is a non-invasive procedure, which is desirable in many cases. Another aspect of using fiber sensors in textiles is weaving the fibers into braces to monitor the pressure between the brace and the body of a scoliosis patient [131]. During MRI examination, fiber-optic sensors are probably the only choice to monitor respiration and heart activity because the sensors are immune to electromagnetic interference. For this specific application, measurement errors for respiration and heart rates within 7% were demonstrated by Dziuda et al. [132]. Figure 6 schematically shows the configurations of fiber sensors used in health-care monitoring, where the sensors are embedded in braces that patients can wear easily. Typically, respiration and heart rates can be monitored precisely using the brace. Such a brace with sensors also helps to give pressure feedback to doctors when treating scoliosis patients. A detailed pressure distribution and statistics during recovery can be obtained from a patient wearing a smart brace. An FBG sensor on the wrist could provide better analysis of blood pressure, as demonstrated in [133]. Moreover, as shown in Figure 6b, interferometry-based fiber sensors integrated inside a mattress could monitor health condition during sleeping, providing heart and respiration rates as well as the status of lying in bed or leaving the bed [134,135]. This information is important for the elderly or for patients with sleep apnea hypopnea syndrome.

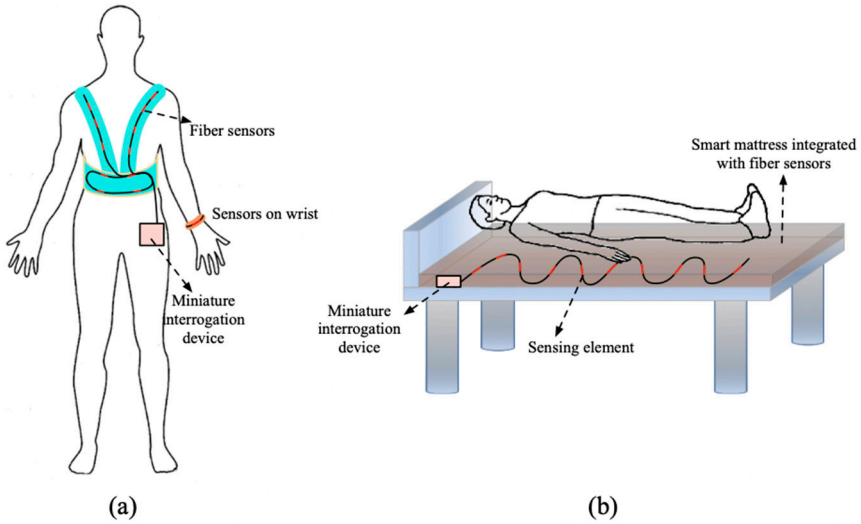

Figure 6. Schematic demonstrating health-care monitoring based on optical fiber sensors, where (**a**) shows sensor devices in a brace and a bracelet to monitor heart condition, blood pressure, and respiration, (**b**) illustrates a smart mattress integrated with optical fiber sensors to monitor health condition during sleeping, e.g., heart and respiration rates and the status of lying in bed or leaving the bed.

Using a single FBG sensor, Silva et al. have demonstrated a simultaneous cardiac and respiratory frequency measurement by embedding the sensor in polymeric foil [136]. The quality of the results was determined by comparing the detection system and a commercial device. Blood pressure can be measured using FBG sensors, as demonstrated by a group at Shinshu University [133,137,138]. It has been shown that systolic and diastolic blood pressure can be characterized by attaching a single FBG across the wrist [133]. Basically, the slight force induced by pulsing blood flow in the vessel is measured by the FBG. A partial least-squares regression algorithm was constructed to predict blood pressure using the pulse wave detected by the FBG. It is very promising that only one silica FBG can monitor the tiny change caused by the blood pulse wave. Recently, a similar measurement was demonstrated using POF gratings [139]. An approximately 20-fold improvement in sensitivity was achieved due to the much lower Young's modulus of POF compared with silica glass. This provides a better option for blood pressure measurement. As expected for this particular application, the algorithm and system would be simpler using POFs. Polymers, including PMDS or other hydrogels, are softer, and therefore better performance could be obtained by polymer sensor-based physical strain detection.

Fabrics integrated with PMMA multimode fiber loops with a notch were demonstrated to be good large strain sensors up to 30% strain [140]. They have been used for respiration monitoring [141]. As a cool light source, side-emitting POFs were woven into flexible fabrics as wearable phototherapy devices [142,143], showing promise for treatment of conditions such as neonatal Jaundice.

Moreover, to benefit from its flexibility and biocompatibility, hydrogel-based optical fiber could possibly be implanted inside tissue to measure glucose. A demonstration of p(PEDGA) fiber implanted in porcine tissue has been reported [49]. Promising development of hydrogel optical fiber sensors for blood glucose is anticipated.

7. Conclusions

This paper has presented a review of multi-material-based specialty optical fibers. In particular, optical fibers made of silica glass, soft glass, PMMA, biomaterials, hydrogel, PDMS, CYTOP, chalcogenide multi-materials, metals, and inorganic components have been reviewed. The various fabrication methods used to make these multifunctional fibers have been summarized, typically including casting, drilling, extrusion, and stacking. Microstructures providing more functions and greater flexibility in development of fiber devices have been introduced. The widely used fiber Bragg grating (FBG) technique is presented in terms of its sensing principle and fabrication. Interferometric sensing techniques have been summarized as well. When using these approaches, multi-material-based fibers are a good platform to develop high-performance sensors because more material options are available. By introducing metals or semiconductors into the fibers, novel photonic devices (e.g., fiber capacitors or modulators) are possible. Lastly, typical sensing applications based on specialty optical fibers in the oil and gas industry, optofluidics, and health monitoring have been described. All these applications benefit from the flexibility of specialty optical fibers in materials and structures. In contrast to the conventional silica glass fibers typically developed for telecommunication, these multi-material, micro-structured optical fibers provide more functions, especially in sensing applications.

As for future prospects, soft glass-based fibers could attract increasing attention by combining different materials with the glass. Chalcogenide and tellurite glasses are good substrates to integrate other metals or inorganic materials, making them prized in the fabrication of multi-material fibers. Because even a tiny variation in the components of these materials leads to large changes in fiber properties, fully characterizing fiber devices is challenging. The other aspect of introducing and integrating different materials is compatibility, which determines whether the multi-material preform is drawable. This concern is more urgent when the two materials have significantly different thermal properties, for example, glass and metals or glass and other inorganic elements. Normally, using the traditional drawing approach, the fiber material should possess good tactility, and the two materials should have similar thermal expansion coefficients. Otherwise, cracks or bubbles occur randomly

along the fiber length, which is not desirable for fiber devices. The proper combination of multiple materials is a scientific issue, and better fabrication techniques for optical fibers are under investigation.

Apart from the glasses, either silica or soft-glass, polymer materials have unique characteristics because of their biocompatibility and softness. Many biomedical applications are based on polymer fibers. When polymer materials are drawn into optical fibers, optical detection techniques can be used, for example, light absorption, FBGs, and fiber interferometry. The use of PMMA as a main material to fabricate POFs has been amply demonstrated, and good FBG sensors for physical parameter measurement as well as for medical monitoring have been developed. Other materials such as hydrogels and PDMS are more promising in materials incorporation and in biomedical devices, which could provide a good research direction for designing optical fibers based on polymer materials.

In terms of applications, health monitoring, especially vital signs measurement, is another good direction for using optical fibers regardless of the materials used. By weaving the optical fiber with sensors into textiles, real-time monitoring of a patient's condition is more straightforward and easier to conduct. A brace is one good platform, but smart clothing integrated with a fiber sensing network is promising as well. Wearable devices with fiber sensors monitoring vital signs could push the technology widely into the consumable market, where many people could benefit from it. With the development of Big Data analysis, more information (e.g., stress level) can be retrieved using large amounts of sensing data measured by fiber sensors. In such a potential scenario, high-performance fiber sensors are necessary because the signal for vital signs like blood pressure and pulse is typically very weak. On the other hand, miniature and portable interrogation devices (e.g., chip size) are desirable for wearable sensors. All these topics need further investigations on the basis of multifunctional, multi-material fibers.

Author Contributions: Z.L. and Z.F.Z. co-drafted the manuscript, X.T. initiated and supervised the work, H.-Y.T. supervised the work. All the authors discussed the work and revised the paper.

Funding: Authors would like to acknowledge the financial support of Innovation and Technology Fund, Hong Kong under ITS/306/17, The Hong Kong Polytechnic University under 1-ZVGB, 1-BBYE, 1-BBA3 and 1-BBYS.

Conflicts of Interest: The authors declare no conflict of interest.

References

1. Erdogan, T. Fiber grating spectra. *Light. Technol. J.* **1997**, *15*, 1277–1294. [CrossRef]
2. Kersey, A.D.; Davis, M.A.; Patrick, H.J.; LeBlanc, M.; Koo, K.P.; Askins, C.G.; Putnam, M.A.; Friebele, E.J. Fiber grating sensors. *IEEE J. Light. Technol.* **1997**, *15*, 1442–1463. [CrossRef]
3. Tam, H.Y.; Pun, C.-F.J.; Zhou, G.; Cheng, X.; Tse, M.L.V. Special structured polymer fibers for sensing applications. *Opt. Fiber Technol.* **2010**, *16*, 357–366. [CrossRef]
4. Johnson, I.P.; Kalli, K.; Webb, D.J.; Yuan, W.; Khan, L.; Bang, O.; Rasmussen, H.K.; Stefani, A.; Nielsen, K. Optical fibre Bragg grating recorded in TOPAS cyclic olefin copolymer. *Electron. Lett.* **2011**, *47*, 271. [CrossRef]
5. Woyessa, G.; Fasano, A.; Markos, C.; Stefani, A.; Rasmussen, H.K.; Bang, O. Zeonex micro-structured polymer optical fiber: Fabrication friendly fibers for high temperature and humidity insensitive Bragg grating sensing. *Opt. Mater. Express* **2017**, *7*, 286. [CrossRef]
6. Leber, A.; Cholst, B.; Sandt, J.; Vogel, N.; Kolle, M. Stretchable Thermoplastic Elastomer Optical Fibers for Sensing of Extreme Deformations. *Adv. Funct. Mater.* **2019**, *29*, 1–8. [CrossRef]
7. Choi, M.; Choi, J.W.; Kim, S.; Nizamoglu, S.; Hahn, S.K.; Yun, S.H. Light-guiding hydrogels for cell-based sensing and optogenetic synthesis in vivo. *Nat. Photonics* **2013**, *7*, 987–994. [CrossRef]
8. Le Coq, D.; Boussard-Plédel, C.; Fonteneau, G.; Pain, T.; Bureau, B.; Adam, J.L. Chalcogenide double index fibers: Fabrication, design, and application as a chemical sensor. *Mater. Res. Bull.* **2003**, *38*, 1745–1754. [CrossRef]
9. Zhao, Z.; Wu, B.; Wang, X.; Pan, Z.; Liu, Z.; Zhang, P.; Shen, X.; Nie, Q.; Dai, S.; Wang, R. Mid-infrared supercontinuum covering 2.0–16 μm in a low-loss telluride single-mode fiber. *Laser Photonics Rev.* **2017**, *11*, 2–6. [CrossRef]

10. Zhang, B.; Yu, Y.; Zhai, C.; Qi, S.; Wang, Y.; Yang, A.; Gai, X.; Wang, R.; Yang, Z.; Luther-Davies, B. High Brightness 2.2–12 μm Mid-Infrared Supercontinuum Generation in a Nontoxic Chalcogenide Step-Index Fiber. *J. Am. Ceram. Soc.* **2016**, *4*, 1–4. [CrossRef]
11. Caillaud, C.; Gilles, C.; Provino, L.; Brilland, L.; Jouan, T.; Ferre, S.; Carras, M.; Brun, M.; Mechin, D.; Adam, J.-L.; et al. Highly birefringent chalcogenide optical fiber for polarization-maintaining in the 3–8.5 μm mid-IR window. *Opt. Express* **2016**, *24*, 7977. [CrossRef]
12. Bernier, M.; Fortin, V.; Caron, N.; El-Amraoui, M.; Messaddeq, Y.; Vallée, R. Mid-infrared chalcogenide glass Raman fiber laser. *Opt. Lett.* **2013**, *38*, 127–129. [CrossRef] [PubMed]
13. Egusa, S.; Wang, Z.; Chocat, N.; Ruff, Z.M.; Stolyarov, A.M.; Shemuly, D.; Sorin, F.; Rakich, P.T.; Joannopoulos, J.D.; Fink, Y. Multi-material piezoelectric fibres. *Nat. Mater.* **2010**, *9*, 643–648. [CrossRef]
14. Lee, J.; Khudiyev, T.; Su, H.-W.; Levy, E.; Voldman, J.; Fink, Y.; Yuan, R. Microfluidics in structured multi-material fibers. *Proc. Natl. Acad. Sci. USA* **2018**, *115*, E10830–E10838.
15. Lestoquoy, G.; Chocat, N.; Wang, Z.; Joannopoulos, J.D.; Fink, Y. Fabrication and characterization of thermally drawn fiber capacitors. *Appl. Phys. Lett.* **2013**, *102*, 152908. [CrossRef]
16. Bayindir, M.; Abouraddy, A.F.; Arnold, J.; Joannopoulos, J.D.; Fink, Y. Thermal-sensing fiber devices by multi-material codrawing. *Adv. Mater.* **2006**, *18*, 845–849. [CrossRef]
17. Hill, K.O.; Fujii, Y.; Johnson, D.C.; Kawasaki, B.S. Photosensitivity in optical fiber waveguides: Application to reflection filter fabrication. *Appl. Phys. Lett.* **1978**, *32*, 647. [CrossRef]
18. Moulton, P.F.; Rines, G.A.; Slobodtchikov, E.V.; Wall, K.F.; Frith, G.; Samson, B.; Carter, A.L.G. Tm-doped fiber lasers: Fundamentals and power scaling. *IEEE J. Sel. Top. Quantum Electron.* **2009**, *15*, 85–92. [CrossRef]
19. Arai, K.; Namikawa, H.; Kumata, K.; Honda, T.; Ishii, Y.; Handa, T. Aluminum or phosphorus co-doping effects on the fluorescence and structural properties of neodymium-doped silica glass. *J. Appl. Phys.* **1986**, *59*, 3430–3436. [CrossRef]
20. Ramírez-Martínez, N.J.; Núñez-Velázquez, M.; Umnikov, A.A.; Sahu, J.K. Highly efficient thulium-doped high-power laser fibers fabricated by MCVD. *Opt. Express* **2019**, *27*, 196. [CrossRef]
21. Russell, P. Photonic crystal fibers. *Science* **2003**, *299*, 358–362. [CrossRef]
22. Russell, P.S.J. Photonic-Crystal Fibers. *J. Light. Technol.* **2006**, *24*, 4729–4749.
23. Tanaka, K.; Toyosawa, N.; Hisakuni, H. Photoinduced Bragg gratings in As_2S_3 optical fibers. *Opt. Lett.* **1995**, *20*, 1976–1978. [CrossRef] [PubMed]
24. Ahmad, R.; Rochette, M.; Baker, C. Fabrication of Bragg gratings in subwavelength diameter As_2Se_3 chalcogenide wires. *Opt. Lett.* **2011**, *36*, 2886–2888. [CrossRef]
25. Zhao, Z.; Wang, X.; Dai, S.; Pan, Z.; Liu, S.; Sun, L.; Zhang, P.; Liu, Z.; Nie, Q.; Shen, X.; et al. 1.5–14 μm midinfrared supercontinuum generation in a low-loss Te-based chalcogenide step-index fiber. *Opt. Lett.* **2016**, *41*, 5222–5225. [CrossRef]
26. Hartouni, E.; Mecholsky, J.J. Mechanical Properties of Chalcogenide Glasses. In *Proceedings Volume 0683, Infrared and Optical Transmitting Materials*; Schwartz, R.W., Ed.; SPIE: Bellingham, WA, USA, 1986; Volume I, p. 92.
27. Lucas, P.; Riley, M.R.; Boussard-Plédel, C.; Bureau, B. Advances in chalcogenide fiber evanescent wave biochemical sensing. *Anal. Biochem.* **2006**, *351*, 1–10. [CrossRef]
28. Bureau, B.; Boussard, C.; Cui, S.; Chahal, R.; Anne, M.L.; Nazabal, V.; Sire, O.; Loréal, O.; Lucas, P.; Monbet, V.; et al. Chalcogenide optical fibers for mid-infrared sensing. *Opt. Eng.* **2014**, *53*, 027101. [CrossRef]
29. Van Popta, A.; Decorby, R.; Haugen, C.; Robinson, T.; McMullin, J.; Tonchev, D.; Kasap, S. Photoinduced refractive index change in As_2Se_3 by 633 nm illumination. *Opt. Express* **2002**, *10*, 639–644. [CrossRef] [PubMed]
30. El-Amraoui, M.; Gadret, G.; Jules, J.C.; Fatome, J.; Fortier, C.; Désévédavy, F.; Skripatchev, I.; Messaddeq, Y.; Troles, J.; Brilland, L.; et al. Micro-structured chalcogenide optical fibers from As_2S_3 glass: Towards new IR broadband sources. *Opt. Express* **2010**, *18*, 26655–26665. [CrossRef]
31. Peng, G.D.; Xiong, Z.; Chu, P.L. Photosensitivity and gratings in dye-doped polymer optical fibers. *Opt. Fiber Technol.* **1999**, *5*, 242–251. [CrossRef]
32. Yu, J.; Tao, X.; Tam, H. Trans-4-stilbenemethanol-doped photosensitive polymer fibers and gratings. *Opt. Lett.* **2004**, *29*, 156–158. [CrossRef] [PubMed]
33. Chen, X.; Zhang, C.; Webb, D.J.; Peng, G.D.; Kalli, K. Bragg grating in a polymer optical fibre for strain, bend and temperature sensing. *Meas. Sci. Technol.* **2010**, *21*, 94005. [CrossRef]

34. Xiong, Z.; Peng, G.D.; Wu, B.; Chu, P.L. Highly Tunable Bragg Gratings in Single-Mode Polymer Optical Fibers. *IEEE Photonics Technol. Lett.* **1999**, *11*, 352–354. [CrossRef]
35. Dobb, H.; Webb, D.J.; Kalli, K.; Argyros, A.; Large, M.C.J.; van Eijkelenborg, M.A. Continuous wave ultraviolet light-induced fiber Bragg gratings in few- and single-mode micro-structured polymer optical fibers. *Opt. Lett.* **2005**, *30*, 3296–3298. [PubMed]
36. Kowal, D.; Statkiewicz-Barabach, G.; Mergo, P.; Urbanczyk, W. Micro-structured polymer optical fiber for long period gratings fabrication using an ultraviolet laser beam. *Opt. Lett.* **2014**, *39*, 2242. [CrossRef] [PubMed]
37. Bundalo, I.-L.; Nielsen, K.; Markos, C.; Bang, O. Bragg grating writing in PMMA micro-structured polymer optical fibers in less than 7 minutes. *Opt. Express* **2014**, *22*, 5270–5276. [CrossRef]
38. Rosenberger, M.; Hellmann, R.; Belle, S.; Schmauss, B.; Hessler, S. TOPAS based humidity insensitive polymer planar Bragg gratings for temperature and multi-axial strain sensing. In *Proceedings Volume 9444, International Seminar on Photonics, Optics, and Its Applications (ISPhOA 2014)*; SPIE: Bellingham, WA, USA, 2015.
39. Choi, M.; Humar, M.; Kim, S.; Yun, S.H. Step-Index Optical Fiber Made of Biocompatible Hydrogels. *Adv. Mater.* **2015**, *27*, 4081–4086. [CrossRef]
40. Guo, J.; Zhou, M.; Yang, C. Fluorescent hydrogel waveguide for on-site detection of heavy metal ions. *Sci. Rep.* **2017**, *7*, 1–8. [CrossRef]
41. Lin, S.; Yuk, H.; Zhang, T.; Parada, G.A.; Koo, H.; Yu, C.; Zhao, X. Stretchable Hydrogel Electronics and Devices. *Adv. Mater.* **2016**, *28*, 4497–4505. [CrossRef]
42. Liu, X.; Yun, S.-H.; Guo, J.; Khademhosseini, A.; Yetisen, A.K.; Yang, C.; Jiang, N.; Yuk, H.; Zhao, X. Highly Stretchable, Strain Sensing Hydrogel Optical Fibers. *Adv. Mater.* **2016**, *28*, 10244–10249.
43. Pathak, A.K.; Singh, V.K. A wide range and highly sensitive optical fiber pH sensor using polyacrylamide hydrogel. *Opt. Fiber Technol.* **2017**, *39*, 43–48. [CrossRef]
44. Parker, S.T.; Domachuk, P.; Amsden, J.; Bressner, J.; Lewis, J.A.; Kaplan, D.L.; Omenetto, F.C. Biocompatible silk printed optical waveguides. *Adv. Mater.* **2009**, *21*, 2411–2415. [CrossRef]
45. Qiao, X.; Qian, Z.; Li, J.; Sun, H.; Han, Y.; Xia, X.; Zhou, J.; Wang, C.; Wang, Y.; Wang, C. Synthetic Engineering of Spider Silk Fiber as Implantable Optical Waveguides for Low-Loss Light Guiding. *Acs Appl. Mater. Interfaces* **2017**, *9*, 14665–14676. [CrossRef]
46. Jain, A.; Yang, A.H.J.; Erickson, D. Gel-based optical waveguides with live cell encapsulation and integrated microfluidics. *Opt. Lett.* **2012**, *37*, 1472. [CrossRef]
47. Rahman, H.A.; Ahmad, H.; Hamida, B.A.; Al-Askari, S.; Harun, S.W.; Irawati, N.; Yasin, M. Relative Humidity Sensing Using a PMMA Doped Agarose Gel Microfiber. *J. Light. Technol.* **2017**, *35*, 3940–3944.
48. Nizamoglu, S.; Gather, M.C.; Humar, M.; Choi, M.; Kim, S.; Kim, K.S.; Hahn, S.K.; Scarcelli, G.; Randolph, M.; Redmond, R.W.; et al. Bioabsorbable polymer optical waveguides for deep-tissue photomedicine. *Nat. Commun.* **2016**, *7*, 1–7. [CrossRef]
49. Yetisen, A.K.; Jiang, N.; Fallahi, A.; Montelongo, Y.; Ruiz-Esparza, G.U.; Tamayol, A.; Zhang, Y.S.; Mahmood, I.; Yang, S.A.; Kim, K.S.; et al. Glucose-Sensitive Hydrogel Optical Fibers Functionalized with Phenylboronic Acid. *Adv. Mater.* **2017**, *29*, 1606380. [CrossRef]
50. Jiang, N.; Ahmed, R.; Rifat, A.A.; Guo, J.; Yin, Y.; Montelongo, Y.; Butt, H.; Yetisen, A.K. Functionalized Flexible Soft Polymer Optical Fibers for Laser Photomedicine. *Adv. Opt. Mater.* **2018**, *6*, 1–10. [CrossRef]
51. Liu, Z.; Kim, G.B.; Kalaba, S.; Zhang, C.; Yang, J.; Mehta, N.; Shan, D. Flexible biodegradable citrate-based polymeric step-index optical fiber. *Biomaterials* **2017**, *143*, 142–148.
52. Sun, Y.L.; Sun, S.M.; Zheng, B.Y.; Hou, Z.S.; Wang, P.; Zhang, X.L.; Dong, W.F.; Zhang, L.; Chen, Q.D.; Tong, L.M.; et al. Protein-Based Multi-Mode Interference Optical Micro-Splitters. *IEEE Photonics Technol. Lett.* **2016**, *28*, 629–632. [CrossRef]
53. Zhao, H.; O'Brien, K.; Li, S.; Shepherd, R.F. Optoelectronically innervated soft prosthetic hand via stretchable optical waveguides. *Sci. Robot.* **2016**, *1*, 1–10. [CrossRef]
54. Harnett, C.K.; Zhao, H.; Shepherd, R.F. Stretchable Optical Fibers: Threads for Strain-Sensitive Textiles. *Adv. Mater. Technol.* **2017**, *2*, 1–7. [CrossRef]
55. Missinne, J.; Van Steenberge, G.; Bosman, E.; Kalathimekkad, S.; Vanfleteren, J.; Van Hoe, B. Stretchable optical waveguides. *Opt. Express* **2014**, *22*, 4168. [CrossRef]
56. Martincek, I.; Pudis, D.; Chalupova, M. Technology for the preparation of PDMS optical fibers and some fiber structures. *IEEE Photonics Technol. Lett.* **2014**, *26*, 1446–1449. [CrossRef]

57. Abouraddy, A.F.; Bayindir, M.; Benoit, G.; Hart, S.D.; Kuriki, K.; Orf, N.; Shapira, O.; Sorin, F.; Temelkuran, B.; Fink, Y. Towards multi-material multifunctional fibres that see, hear, sense and communicate. *Nat. Mater.* **2007**, *6*, 336–347. [CrossRef] [PubMed]
58. Temelkuran, B.; Hart, S.D.; Benoit, G.; Joannopoulos, J.D.; Fink, Y. Wavelength-scalable hollow optical fibres with large photonic bandgaps for CO_2 laser transmission. *Nature* **2002**, *420*, 650–653. [CrossRef] [PubMed]
59. Viens, J.F.; Hart, S.D.; Benoit, G.; Bayindir, M.; Shapira, O.; Kuriki, K.; Kuriki, Y.; Joannopoulos, J.D.; Fink, Y. Hollow multilayer photonic bandgap fibers for NIR applications. *Opt. Express* **2004**, *12*, 1510.
60. Hart, S.D.; Maskaly, G.R.; Temelkuran, B.; Prideaux, P.H.; Joannopoulos, J.D.; Fink, Y. External reflection from omnidirectional dielectric mirror fibers. *Science* **2002**, *296*, 510–513. [CrossRef]
61. Benoit, G.; Hart, S.D.; Temelkuran, B.; Joannopoulos, J.D.; Fink, Y. Static and Dynamic Properties of Optical Microcavities in Photonic Bandgap Yarns. *Adv. Mater.* **2003**, *15*, 2053–2056. [CrossRef]
62. Bayindir, M.; Fink, Y.; Sorin, F.; Joannopoulos, J.D.; Hinczewski, D.S.; Arnold, J.; Abouraddy, A.F.; Shapira, O. Large-scale optical-field measurements with geometric fibre constructs. *Nat. Mater.* **2006**, *5*, 532–536.
63. Bayindir, M.; Shapira, O.; Saygin-Hinczewski, D.; Viens, J.; Abouraddy, A.F.; Joannopoulos, J.D.; Fink, Y. Integrated fibres for self-monitored optical transport. *Nat. Mater.* **2005**, *4*, 820–825. [CrossRef]
64. Shapira, O.; Kuriki, K.; Orf, N.D.; Abouraddy, A.F.; Benoit, G.; Viens, J.F.; Rodriguez, A.; Ibanescu, M.; Joannopoulos, J.D.; Fink, Y.; et al. Surface-emitting fiber lasers. *Opt. Express* **2006**, *14*, 3929. [CrossRef]
65. Rein, M.; Favrod, V.D.; Hou, C.; Khudiyev, T.; Stolyarov, A.; Cox, J.; Chung, C.C.; Chhav, C.; Ellis, M.; Joannopoulos, J.; et al. Diode fibres for fabric-based optical communications. *Nature* **2018**, *560*, 214–218. [CrossRef] [PubMed]
66. Hanada, Y.; Sugioka, K.; Midorikawa, K. UV waveguides light fabricated in fluoropolymer CYTOP by femtosecond laser direct writing. *Opt. Express* **2010**, *18*, 446. [CrossRef] [PubMed]
67. Liu, H.Y.; Peng, G.D.; Chu, P.L. Thermal stability of gratings in PMMA and CYTOP polymer fibers. *Opt. Commun.* **2002**, *204*, 151–156. [CrossRef]
68. Lacraz, A.; Polis, M.; Theodosiou, A.; Koutsides, C.; Kalli, K. Femtosecond Laser Inscribed Bragg Gratings in Low Loss CYTOP Polymer Optical Fiber. *IEEE Photonics Technol. Lett.* **2015**, *27*, 693–696. [CrossRef]
69. Jiang, L.; Wang, X.; Guo, F.; Wu, B.; Zhao, Z.; Mi, N.; Li, X.; Dai, S.; Liu, Z.; Nie, Q.; et al. Fabrication and characterization of chalcogenide polarization-maintaining fibers based on extrusion. *Opt. Fiber Technol.* **2017**, *39*, 26–31. [CrossRef]
70. Zhang, B.; Zhai, C.; Qi, S.; Guo, W.; Yang, Z.; Yang, A.; Gai, X.; Yu, Y.; Wang, R.; Tang, D.; et al. High-resolution chalcogenide fiber bundles for infrared imaging. *Opt. Lett.* **2015**, *40*, 4384–4387. [CrossRef]
71. Ebendorff-Heidepriem, H.; Warren-Smith, S. Suspended nanowires: Fabrication, design and characterization of fibers with nanoscale cores. *Opt. Express* **2009**, *17*, 2646–2657. [CrossRef]
72. Liu, B.T.; Chen, W.C.; Hsu, J.P. Mathematical modeling of a co-extrusion process for preparing gradient-index polymer optical fibers. *Polymer* **1999**, *40*, 1451–1457. [CrossRef]
73. Wei, C.; Joseph Weiblen, R.; Menyuk, C.R.; Hu, J. Negative curvature fibers. *Adv. Opt. Photonics* **2017**, *9*, 504. [CrossRef]
74. Hasan, M.I.; Akhmediev, N.; Chang, W. Positive and negative curvatures nested in an antiresonant hollow-core fiber. *Opt. Lett.* **2017**, *42*, 703. [CrossRef]
75. Gattass, R.R.; Rhonehouse, D.; Gibson, D.; McClain, C.; Thapa, R.; Nguyen, V.Q.; Bayya, S.S.; Weiblen, J.; Menyuk, C.R.; Shaw, L.B.; et al. Infrared glass-based negative-curvature anti-resonant fibers fabricated through extrusion. *Opt. Express* **2016**, *24*, 25697–25703. [CrossRef] [PubMed]
76. Birks, T.A.; Knight, J.C.; Russell, P.S. Endlessly single-mode photonic crystal fiber. *Opt. Lett.* **1997**, *22*, 961–963. [CrossRef] [PubMed]
77. Liu, Z.; Tam, H.-Y. Fabrication and Sensing Applications of Special Micro-structured Optical Fibers. In *Selected Topics on Optical Fiber Technologies and Applications*; Xu, F., Mou, C., Eds.; InTech: London, UK, 2018; pp. 1–20. ISBN 978-953-51-3813-6.
78. Liu, Z.; Wu, C.; Tse, M.-L.V.; Tam, H.-Y. Fabrication, Characterization, and Sensing Applications of a High-Birefringence Suspended-Core Fiber. *J. Light. Technol.* **2014**, *32*, 2113–2122. [CrossRef]
79. Liu, Z.; Htein, L.; Lee, K.-K.; Lau, K.-T.; Tam, H.-Y. Large dynamic range pressure sensor based on two semicircle-holes micro-structured fiber. *Sci. Rep.* **2018**, *8*, 65. [CrossRef]

80. Anuszkiewicz, A.; Statkiewicz-Barabach, G.; Borsukowski, T.; Olszewski, J.; Martynkien, T.; Urbanczyk, W.; Mergo, P.; Makara, M.; Poturaj, K.; Geernaert, T.; et al. Sensing characteristics of the rocking filters in micro-structured fibers optimized for hydrostatic pressure measurements. *Opt. Express* **2012**, *20*, 23320. [CrossRef]
81. Tse, M.-L.V.; Liu, Z.; Cho, L.-H.; Lu, C.; Wai, P.-K.A.; Tam, H. Superlattice Micro-structured Optical Fiber. *Materials* **2014**, *7*, 4567–4573. [CrossRef] [PubMed]
82. Htein, L.; Liu, Z.; Gunawardena, D.; Tam, H.-Y.Y. Single-ring suspended fiber for Bragg grating based hydrostatic pressure sensing. *Opt. Express* **2019**, *27*, 9655. [CrossRef] [PubMed]
83. Zhang, A.P.; Guan, B.O.; Tao, X.-M.; Tam, H.Y. Experimental and theoretical analysis of fiber Bragg gratings under lateral compression. *Opt. Commun.* **2002**, *206*, 81–87. [CrossRef]
84. Zhang, A.P.; Guan, B.-O.; Tao, X.-M.; Tam, H.Y. Mode couplings in superstructure fiber Bragg gratings. *IEEE Photonics Technol. Lett.* **2002**, *14*, 489–491. [CrossRef]
85. Du, W.-C.; Tao, X.-M.; Tam, H.-Y. Fiber Bragg grating cavity sensor for simultaneous measurement of strain and temperature. *IEEE Photonics Technol. Lett.* **1999**, *11*, 105–107.
86. Du, W.; Tao, X.; Tam, H.-Y. Temperature independent strain measurement with a fiber grating tapered cavity sensor. *Photonics Technol. Lett. IEEE* **1999**, *11*, 596–598.
87. Zhang, A.-P.; Tao, X.-M.; Chung, W.-H.; Guan, B.-O.; Tam, H.-Y. Cladding-mode-assisted recouplings in concatenated long-period and fiber Bragg gratings. *Opt. Lett.* **2002**, *27*, 1214. [CrossRef] [PubMed]
88. Guan, B.O.; Zhang, A.P.; Tam, H.Y.; Chan, H.L.; Choy, C.L.; Tao, X.M.; Demokan, M.S. Step-changed long-period fiber gratings. *IEEE Photonics Technol. Lett.* **2002**, *14*, 657–659. [CrossRef]
89. Chi, H.; Tao, X.-M.; Yang, D.-X.; Chen, K.-S. Simultaneous measurement of axial strain, temperature, and transverse load by a superstructure fiber grating. *Opt. Lett.* **2007**, *26*, 1949. [CrossRef]
90. Malo, B.; Albert, J.; Hill, K.O.; Bilodeau, F.; Johnson, D.C. Effective index drift from molecular nydrogen dizusion in hydrogen-loaded optical fibres and its effect on Bragg grating fabrication. *Electron. Lett.* **1994**, *30*, 1727–1729. [CrossRef]
91. Hill, K.O.; Meltz, G. Fiber Bragg grating technology fundamentals and overview. *J. Light. Technol.* **1997**, *15*, 1263–1276. [CrossRef]
92. Ran, Y.; Tan, Y.-N.; Sun, L.-P.; Gao, S.; Li, J.; Jin, L.; Guan, B.-O. 193 nm excimer laser inscribed Bragg gratings in microfibers for refractive index sensing. *Opt. Express* **2011**, *19*, 18577–18583. [CrossRef]
93. Gagné, M.; Kashyap, R. New nanosecond Q-switched 213 and 224 nm lasers for fiber Bragg grating inscription in hydrogen-free fibers. *Laser Appl. Microelectron. Optoelectron. Manuf. XVII* **2012**, *8243*, 824314.
94. Marques, C.A.F.; Min, R.; Leal Junior, A.; Antunes, P.; Fasano, A.; Woyessa, G.; Nielsen, K.; Rasmussen, H.K.; Ortega, B.; Bang, O. Fast and stable gratings inscription in POFs made of different materials with pulsed 248 nm KrF laser. *Opt. Express* **2018**, *26*, 2013. [CrossRef]
95. Cui, W.; Chen, T.; Si, J.; Chen, F.; Hou, X. Femtosecond laser processing of fiber Bragg gratings with photo-induced gradient-index assisted focusing. *J. Micromech. Microeng.* **2014**, *24*, 075015. [CrossRef]
96. Baghdasaryan, T.; Geernart, T.; Morana, A.; Marin, E.; Girard, S.; Makara, M.; Mergo, P.; Thienpont, H.; Berghmans, F. IR femtosecond pulsed laser-based fiber Bragg grating inscription in a photonic crystal fiber using a phase mask and a short focal length lens. *Opt. Express* **2018**, *26*, 14741. [CrossRef]
97. Elsmann, T.; Habisreuther, T.; Graf, A.; Rothhardt, M.; Bartelt, H. Inscription of first-order sapphire Bragg gratings using 400 nm femtosecond laser radiation. *Opt. Express* **2013**, *21*, 4591. [CrossRef]
98. Thomas, J.U.; Jovanovic, N.; Krämer, R.G.; Marshall, G.D.; Withford, M.J.; Tünnermann, A.; Nolte, S.; Steel, M.J. Cladding mode coupling in highly localized fiber Bragg gratings II: Complete vectorial analysis. *Opt. Express* **2012**, *20*, 21434. [CrossRef] [PubMed]
99. Waltermann, C.; Doering, A.; Köhring, M.; Angelmahr, M.; Schade, W. Cladding waveguide gratings in standard single-mode fiber for 3D shape sensing. *Opt. Lett.* **2015**, *40*, 3109. [CrossRef] [PubMed]
100. Wu, C.; Fu, H.Y.; Qureshi, K.K.; Guan, B.-O.; Tam, H.Y. High-pressure and high-temperature characteristics of a Fabry-Perot interferometer based on photonic crystal fiber. *Opt. Lett.* **2011**, *36*, 412–414. [CrossRef] [PubMed]
101. Ke, T.; Zhu, T.; Rao, Y.; Deng, M. Accelerometer based on all-fiber Fabry–Pérot interferometer formed by hollow-core photonic crystal fiber. *Microw. Opt. Technol. Lett.* **2010**, *52*, 2531–2535. [CrossRef]
102. Kim, B.; Kim, T.-H.; Cui, L.; Chung, Y. Twin core photonic crystal fiber for in-line Mach-Zehnder interferometric sensing applications. *Opt. Express* **2009**, *17*, 15502–15507. [CrossRef]

103. Chen, D.; Wu, C.; Tse, M. Hydrostatic Pressure Sensor Based on Mode Interference of a Few Mode Fiber. *Prog. Electromagn.* **2011**, *119*, 335–343. [CrossRef]
104. Ortigosa-Blanch, A.; Knight, J.; Wadsworth, W. Highly birefringent photonic crystal fibers. *Opt. Lett.* **2000**, *25*, 1325–1327. [CrossRef] [PubMed]
105. Suzuki, K.; Kubota, H.; Kawanishi, S.; Tanaka, M.; Fujita, M. Optical properties of a low-loss polarization-maintaining photonic crystal fiber. *Opt. Express* **2001**, *9*, 676–680. [CrossRef] [PubMed]
106. Fini, J.M.; Nicholson, J.W.; Mangan, B.; Meng, L.; Windeler, R.S.; Monberg, E.M.; DeSantolo, A.; DiMarcello, F.V.; Mukasa, K. Polarization maintaining single-mode low-loss hollow-core fibres. *Nat. Commun.* **2014**, *5*, 1–7. [CrossRef] [PubMed]
107. Szpulak, M.; Statkiewicz, G.; Olszewski, J.; Martynkien, T.; Urbańczyk, W.; Wójcik, J.; Makara, M.; Klimek, J.; Nasilowski, T.; Berghmans, F.; et al. Experimental and theoretical investigations of birefringent holey fibers with a triple defect. *Appl. Opt.* **2005**, *44*, 2652–2658. [CrossRef]
108. Xu, M.; Reekie, L.; Chow, Y.; Dakin, J.P. Optical in-fibre grating high pressure sensor. *Electron. Lett.* **1993**, *29*, 398–399. [CrossRef]
109. Wu, C.; Guan, B.-O.; Wang, Z.; Feng, X. Characterization of Pressure Response of Bragg Gratings in Grapefruit Micro-structured Fibers. *J. Light. Technol.* **2010**, *28*, 1392–1397.
110. Bhowmik, K.; Peng, G.-D.; Luo, Y.; Ambikairajah, E.; Lovric, V.; Walsh, W.R.; Rajan, G. Experimental Study and Analysis of Hydrostatic Pressure Sensitivity of Polymer Fibre Bragg Gratings. *J. Light. Technol.* **2015**, *33*, 2456–2462. [CrossRef]
111. Available online: http://www2.emersonprocess.com/en-IN/news/pr/Pages/509-Roxar.aspx (accessed on 1 March 2019).
112. Fu, H.Y.; Tam, H.Y.; Shao, L.-Y.; Dong, X.; Wai, P.K.A.; Lu, C.; Khijwania, S.K. Pressure sensor realized with polarization-maintaining photonic crystal fiber-based Sagnac interferometer. *Appl. Opt.* **2008**, *47*, 2835–2839. [CrossRef]
113. Anuszkiewicz, A.; Martynkien, T.; Mergo, P.; Makara, M.; Urbanczyk, W. Sensing and transmission characteristics of a rocking filter fabricated in a side-hole fiber with zero group birefringence. *Opt. Express* **2013**, *21*, 12657. [CrossRef]
114. Zhang, Z.F.; Tao, X.M.; Zhang, H.P.; Zhu, B. Soft fiber optic sensors for precision measurement of shear stress and pressure. *IEEE Sens. J.* **2013**, *13*, 1478–1482. [CrossRef]
115. Chmielewska, E.; Urbańczyk, W.; Bock, W.J. Measurement of pressure and temperature sensitivities of a Bragg grating imprinted in a highly birefringent side-hole fiber. *Appl. Opt.* **2003**, *42*, 6284–6291. [CrossRef] [PubMed]
116. Song, D.; Wei, Z.; Zou, J.; Yang, S.; Du, E.; Cui, H. Pressure Sensor Based on Fiber Bragg Grating and Carbon Fiber Ribbon-Wound Composite Cylindrical Shell. *Sens. J.* **2009**, *9*, 828–831. [CrossRef]
117. Johnson, I.P.; Webb, D.J.; Kalli, K. Hydrostatic pressure sensing using a polymer optical fibre Bragg gratings. In Proceedings of the Third Asia Pacific Optical Sensors Conference, Sydney, Australia, 31 Janunary–3 February 2012; Volume 8351, p. 835106.
118. Sulejmani, S.; Sonnenfeld, C.; Geernaert, T.; Mergo, P.; Makara, M.; Poturaj, K.; Skorupski, K.; Martynkien, T.; Statkiewicz-Barabach, G.; Olszewski, J.; et al. Control over the pressure sensitivity of Bragg grating-based sensors in highly birefringent micro-structured optical fibers. *IEEE Photonics Technol. Lett.* **2012**, *24*, 527–529. [CrossRef]
119. Liu, Z.; Tse, M.-L.V.; Wu, C.; Chen, D.; Lu, C.; Tam, H.-Y. Intermodal coupling of supermodes in a twin-core photonic crystal fiber and its application as a pressure sensor. *Opt. Express* **2012**, *20*, 21749. [CrossRef] [PubMed]
120. Sadeghi, J.; Latifi, H.; Murawski, M.; Mirkhosravi, F.; Nasilowski, T.; Mergo, P.; Poturaj, K. Group polarimetric pressure sensitivity of an elliptical-core side-hole fiber at telecommunication wavelengths. *IEEE J. Sel. Top. Quantum Electron.* **2016**, *22*, 49–54. [CrossRef]
121. Osório, J.H.; Chesini, G.; Serrão, V.A.; Franco, M.A.R.; Cordeiro, C.M.B. Simplifying the design of micro-structured optical fibre pressure sensors. *Sci. Rep.* **2017**, *7*, 2990. [CrossRef] [PubMed]
122. Lien, V.; Vollmer, F. Microfluidic flow rate detection based on integrated optical fiber cantilever. *Lab Chip* **2007**, *7*, 1352–1356. [CrossRef]
123. Minzioni, P.; Osellame, R.; Sada, C.; Zhao, S.; Omenetto, F.G.; Gylfason, K.B.; Haraldsson, T.; Zhang, Y.; Ozcan, A.; Wax, A.; et al. Roadmap for optofluidics. *J. Opt.* **2017**, *19*, 093003. [CrossRef]

124. Wu, C.; Tse, M.-L.V.; Liu, Z.; Guan, B.-O.; Lu, C.; Tam, H.-Y. In-line microfluidic refractometer based on C-shaped fiber assisted photonic crystal fiber Sagnac interferometer. *Opt. Lett.* **2013**, *38*, 3283–3286. [CrossRef]
125. Ertman, S.; Lesiak, P.; Wolinski, T.R. Optofluidic Photonic Crystal Fiber-Based Sensors. *J. Light. Technol.* **2017**, *35*, 3399–3405. [CrossRef]
126. Unterkofler, S.; McQuitty, R.J.; Euser, T.G.; Farrer, N.J.; Sadler, P.J.; Russell, P.S.J. Microfluidic integration of photonic crystal fibers for online photochemical reaction analysis. *Opt. Lett.* **2012**, *37*, 1952–1954. [CrossRef]
127. Ponce, S.; Munoz, M.; Cubillas, A.M.; Euser, T.G.; Zhang, G.-R.; Russell, P.S.J.; Wasserscheid, P.; Etzold, B.J.M. Stable Immobilization of Size-Controlled Bimetallic Nanoparticles in Photonic Crystal Fiber Microreactor. *Chem. Ing. Tech.* **2018**, *90*, 653–659. [CrossRef]
128. Gao, R.; Lu, D.F.; Cheng, J.; Jiang, Y.; Jiang, L.; Xu, J.D.; Qi, Z.M. Fiber optofluidic biosensor for the label-free detection of DNA hybridization and methylation based on an in-line tunable mode coupler. *Biosens. Bioelectron.* **2016**, *86*, 321–329. [CrossRef]
129. Leite, I.T.; Turtaev, S.; Jiang, X.; Šiler, M.; Cuschieri, A.; Russell, P.S.J.; Čižmár, T. Three-dimensional holographic optical manipulation through a high-numerical-aperture soft-glass multimode fibre. *Nat. Photonics* **2017**, *12*, 1–7. [CrossRef]
130. Massaroni, C.; Saccomandi, P.; Schena, E. Medical smart textiles based on fiber optic technology: An overview. *J. Funct. Biomater.* **2015**, *6*, 204–221. [CrossRef]
131. Wong, M.-S.; Zhao, V.H.; Lou, E.; Chalmers, E.; Hill, D. Development of a Pressure Control System for Brace Treatment of Scoliosis. *IEEE Trans. Neural Syst. Rehabil. Eng.* **2012**, *20*, 557–563.
132. Dziuda, Ł.; Skibniewski, F.W.; Krej, M.; Baran, P.M. Fiber Bragg grating-based sensor for monitoring respiration and heart activity during magnetic resonance imaging examinations. *J. Biomed. Opt.* **2013**, *18*, 057006. [CrossRef]
133. Katsuragawa, Y.; Ishizawa, H. Non-invasive Blood Pressure Measurement by Pulse Wave Analysis Using FBG Sensor. In Proceedings of the 2015 IEEE International Instrumentation and Measurement Technology Conference (I2MTC), Pisa, Italy, 11–14 May 2015; pp. 511–515.
134. Chen, S.; Huang, Z.; Tan, F.; Yang, T.; Tu, J.; Yu, C. Vital signs monitoring using few-mode fiber-based sensors. In Proceedings of the Photonics ASIA 2018, Beijing, China, 11–13 October 2018; p. 108140P.
135. Chen, S.; Tan, F.; Huang, Z.; Yang, T.; Tu, J.; Yu, C. Non-invasive smart monitoring system based on multi-core fiber optic interferometers. In Proceedings of the 2018 IEEE Asia Communications and Photonics Conference (ACP), Hangzhou, China, 26–29 October 2018; pp. 1–3.
136. Silva, A.F.; Carmo, J.P.; Mendes, P.M.; Correia, J.H. Simultaneous cardiac and respiratory frequency measurement based on a single fiber Bragg grating sensor. *Meas. Sci. Technol.* **2011**, *22*, 75801. [CrossRef]
137. Miyauchi, Y.; Koyama, S.; Ishizawa, H. Basic experiment of blood-pressure measurement which uses FBG sensors. In Proceedings of the 2013 IEEE International Instrumentation and Measurement Technology Conference (I2MTC), Minneapolis, MN, USA, 6–9 May 2013; pp. 1767–1770.
138. Miyauchi, Y.; Ishizawa, H.; Koyama, S.; Sato, S. Verification of the systolic blood-pressure measurement principle by FBG sensors. In Proceedings of the 2012 SICE Annual Conference (SICE), Akita, Japan, 20–23 August 2012; pp. 619–622.
139. Bonefacino, J.; Tam, H.Y.; Glen, T.S.; Cheng, X.; Pun, C.J.; Wang, J.; Lee, P.; Tse, M.V.; Boles, S.T. Ultra-fast polymer optical fibre Bragg grating inscription for medical devices. *Light Sci. Appl.* **2018**, *7*, 17161. [CrossRef] [PubMed]
140. Ying, D.Q.; Tao, X.M.; Zheng, W.; Wang, G.F. Fabric strain sensor integrated with looped polymeric optical fiber with large angled V-shaped notches. *Smart Mater. Struct.* **2013**, *22*, 015004. [CrossRef]
141. Zheng, W.; Tao, X.; Zhu, B.; Wang, G.; Hui, C. Fabrication and evaluation of a notched polymer optical fiber fabric strain sensor and its application in human respiration monitoring. *Text. Res. J.* **2014**, *84*, 1791–1802. [CrossRef]

142. Shen, J.; Chui, C.; Tao, X. Luminous fabric devices for wearable low-level light therapy. *Biomed. Opt. Express* **2013**, *4*, 2925. [CrossRef]
143. Shen, J.; Tao, X.; Ying, D.; Hui, C.; Wang, G. Light-emitting fabrics integrated with structured polymer optical fibers treated with an infrared CO_2 laser. *Text. Res. J.* **2013**, *83*, 730–739. [CrossRef]